An efficient time-lapse full waveform inversion by saving the wavefield at boundaries around the reservoir

Yinbin Ma and Robert G. Clapp

ABSTRACT

The need to propagate the source and receiver wavefield over the whole subsurface model is a challenge for time-lapse full-waveform inversion (FWI). We show that by saving the wavefield at the boundary enclosing the reservoir, we can estimate the wavefield around the reservoir after model perturbation. The perturbed wavefield can predict synthetic data at the surface through the precomputed Green's function. We eliminate the need to propagate the wavefield through the overburden area and therefore accelerate the FWI procedure. Random phase-encoding can be incorporated into our proposed workflow and has the potential to further reduce the computational cost.

INTRODUCTION

Full-waveform inversion (Tarantola, 1984; Virieux and Operto, 2009) estimates the high-resolution subsurface models by minimizing the mismatch between the observed data and the synthetic data. FWI is a useful tool for time-lapse (4D) seismic imaging problems (Maharramov and Biondi, 2013). One of the computational challenges of time-lapse FWI is that we need to propagate the source and receiver wavefield through the whole subsurface model several times for each FWI iteration. This computational cost limits the number of iterations we can afford and therefore reduces the quality of 4D FWI results.

Previous studies (Robertsson and Chapman, 2000; Clapp, 2008; Borisov and Singh, 2013; Willemsen et al., 2016) show that by saving the wavefield at the boundaries of the computational domain, the wavefield inside the boundaries can be regenerated. Based on this idea, Clapp (2008) developed memory efficient reverse-time migration (RTM), and Robertsson and Chapman (2000) proposed an efficient algorithm for computing synthetic seismograms after model alternation. In this paper, we study the feasibility of accelerating time-lapse FWI by reconstructing the wavefield near the reservoir using similar techniques.

First we show that by saving the wavefield at the boundaries enclosing the reservoir, we can reconstruct the background wavefield and compute the perturbed wavefield. The wavefield within the boundaries is regenerated by injecting the saved

boundaries, with the computational domain being the enclosed area which is much smaller than the whole subsurface model. The perturbed wavefield can predict the synthetic data at the surface with the pre-computed Green's function, without numerical wave propagation in the overburden area. Therefore FWI procedure is accelerated and more iterations are affordable.

Memory requirements and computational cost increase with the size of the seismic data, as the wavefield for each shot has to be saved. We aim to further reduce the computational cost by incorporating random phase-encoding (Tang, 2011) into our workflow.

METHODS

The FWI objection function measures the mismatch between the synthetic data and the recorded data,

$$J(\mathbf{m}) = \frac{1}{2}\|\mathbf{d}^{\text{syn}}(\mathbf{m}) - \mathbf{d}^{\text{obs}}\|_2^2, \tag{1}$$

where $\mathbf{m}$ is the subsurface model we want to estimate (velocity, anisotropic parameters, elastic parameters, etc), $\mathbf{d}^{\text{syn}}$ is the synthetic data obtained by forward propagating the source wavefield, and $\mathbf{d}^{\text{obs}}$ is the recorded data during the seismic survey. To minimize this objective function 1, the adjoint-state methods are commonly used (Tromp et al., 2005; Plessix, 2006), which require the backward propagation of the data residuals $\left(\mathbf{d}^{\text{syn}}(\mathbf{m}) - \mathbf{d}^{\text{obs}}\right)$.

For time-lapse FWI we are mostly interested in estimating production-induced model change in the vicinity of the reservoir. In comparison, there is little change in the overburden model during production. Direct application of the adjoint-state methods is computationally expensive as it requires wave propagations through the overburden area at every iteration. To reduce the cost, we modify the previous objective function, assuming the overburden has been estimated properly,

$$\begin{aligned} J(\mathbf{m}) &= \frac{1}{2}\| \left(\mathbf{d}^{\text{syn}}(\mathbf{m}) - \mathbf{d}^{\text{syn}}(\mathbf{m_0})\right) - \left(\mathbf{d}_{\text{obs}} - \mathbf{d}^{\text{syn}}(\mathbf{m_0})\right) \|_2^2 \\ &= \frac{1}{2}\|\tilde{\mathbf{d}}^{\text{syn}}(\mathbf{m}) - \tilde{\mathbf{d}}_{\text{obs}}\|_2^2, \end{aligned} \tag{2}$$

where $\mathbf{m_0}$ is the background subsurface model, and $\tilde{\mathbf{d}}^{\text{syn}}(\mathbf{m})$ is the perturbed data after model alteration $(\mathbf{m} - \mathbf{m_0})$. We assume $(\mathbf{m} - \mathbf{m_0})$ is non-zero only in the vicinity of the reservoir.

To accelerate the estimation of $\tilde{\mathbf{d}}^{\text{syn}}(\mathbf{m})$, we can set up virtual receivers at the top of the reservoir (as indicated in Figure 1), and record the perturbed wavefield $\tilde{\mathbf{p}}^{\text{syn}}(\mathbf{m})$. The perturbed data at the surface can then be predicted from the perturbed wavefield at the virtual receivers as,

$$\tilde{\mathbf{d}}^{\text{syn}}(\mathbf{m}) = \mathbf{G}\tilde{\mathbf{p}}^{\text{syn}}(\mathbf{m}), \tag{3}$$

where $\mathbf{G}$ is the pre-computed Green's function thats connect the virtual receivers to the surface receivers. $\mathbf{G}$ is a linear operator. Hence our new objection function can be rewritten as,

$$J(\mathbf{m}) = \frac{1}{2}\|\mathbf{G}\tilde{\mathbf{p}}^{\text{syn}}(\mathbf{m}) - \mathbf{d}^{\text{obs}}\|_2^2. \tag{4}$$

With the new objective function 4, we only need to propagate the wavefield to the virtual receivers instead of all the way to the surface. The wavefield $\tilde{\mathbf{p}}^{\text{syn}}(\mathbf{m})$ can be compute efficiently with the following wave equation (acoustic wave equation for example),

$$\begin{aligned} \left[\mathbf{m}\partial_t^2 - \nabla^2\right] \mathbf{p}^{\text{syn}}(\mathbf{m}) &= 0, \\ \mathbf{p}^{\text{syn}}(\mathbf{m}) &= \mathbf{p}^{\text{syn}}_{\text{saved}}, \text{ in boundary area B} \\ \tilde{\mathbf{p}}^{\text{syn}}(\mathbf{m}) &= \mathbf{p}^{\text{syn}}(\mathbf{m}) - \mathbf{p}^{\text{syn}}(\mathbf{m}_0), \end{aligned} \tag{5}$$

where $\mathbf{p}^{\text{syn}}_{\text{saved}}$ is the saved background wavefield in the boundary area B shown in Fig 1. Notice that equation 5 is different from the initial value problem and numerically we re-inject the saved wavefield in the boundary area. We have eliminated the need to propagate the wave in the overburden area and our algorithm runs faster than the conventional FWI approach.

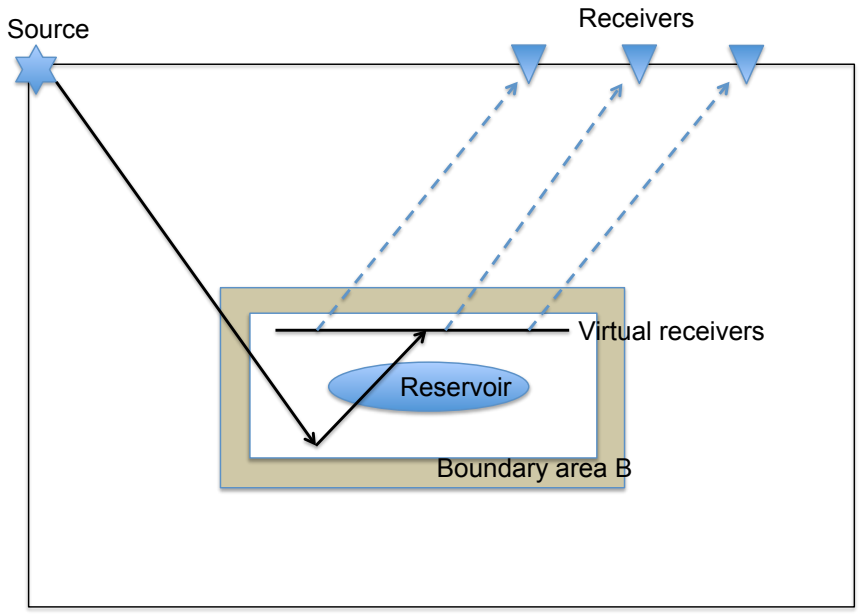

Figure 1: Cartoon illustration of the numerical experiment. The model perturbation is limited to the area within the reservoir. The wavefield in the boudary area B is saved in memory. The perturbed wavefield is numerically estimated near the reservoir and recorded at the virtual receivers. The synthetic data at the surface is estimated from the virtual receivers with the pre-computed Green's function in the overburden area. [**NR**]

The expense of this approach is that we need to save the wavefield at the bound-

aries for every single shot, therefore the memory cost is roughly:

$$\text{memory} \propto N_s \times N_t \times N_b, \tag{6}$$

where N_s is the number of shots in the seismic survey, N_t is the total number of time steps during wave propagation, and N_b is the size of boundaries we need to save. The memory cost is increasing as more shots are included in the FWI objective function.

The memory cost can be further reduce by incorporating the idea of random phase-encoding into our workflow. In equation 1, with $\mathbf{d}^{\text{obs}}$ being the recorded data for all shot, we can write the data in terms of shot gathers $\mathbf{d}^{\text{obs}} = \left[\mathbf{d}_1^{\text{obs}}, \cdots \mathbf{d}_i^{\text{obs}}, \cdots, \mathbf{d}_{N_s}^{\text{obs}}\right]$, with $\mathbf{d}_i^{\text{obs}}$ represent the data for shot i. We can blend the data from different shot,

$$\mathbf{d}^{\text{obs},\alpha} = \frac{1}{\sqrt{N_s}} \sum_{i=1}^{N_s} \mathbf{d}_i^{\text{obs}} \alpha_i, \tag{7}$$

where the weighting function α_i is a complex number and uniformly distributed on the unit circle. has absolute value $|\alpha_i|$.

The new objective function associated with the blended data can be written as,

$$J(\mathbf{m}, \alpha) = \frac{1}{2} \|\mathbf{G}\tilde{\mathbf{p}}^{\text{syn},\alpha}(\mathbf{m}) - \mathbf{d}^{\text{obs},\alpha}\|_2^2, \tag{8}$$

Multiple realizations of phase encoding can be used to attenuate the cross-talk, and our final solution is expressed as,

$$\mathbf{m}^* = \text{argmin}_{\mathbf{m}} \sum_{\alpha=1}^{N_\alpha} J(\mathbf{m}, \alpha), \tag{9}$$

where N_α is the number of realizations of phase encoding. Notice that for equation 9, the memory cost reduces to $\propto N_\alpha \times N_t \times N_b$, which does not grow as the number of shots increase.

NUMERICAL EXAMPLE

Regenerating the wavefield around the reservoir

We design a synthetic model as shown in Figure 2, with a local model perturbation. The wavefield at the boundary area enclosing the reservoir is saved. First we apply equation 5 to the unperturbed model to regenerate the background wavefield. The numerical results can be seen in Figure 3. The wavefield around the reservoir is perfectly regenerated in the absence of model perturbation.

Next we apply equation 5 to perturbed model to predict the perturbed wavefield. The numerical results can be seen in Figure 4. We have captured most of the perturbed wavefield. The difference will be discussed in the following subsection.

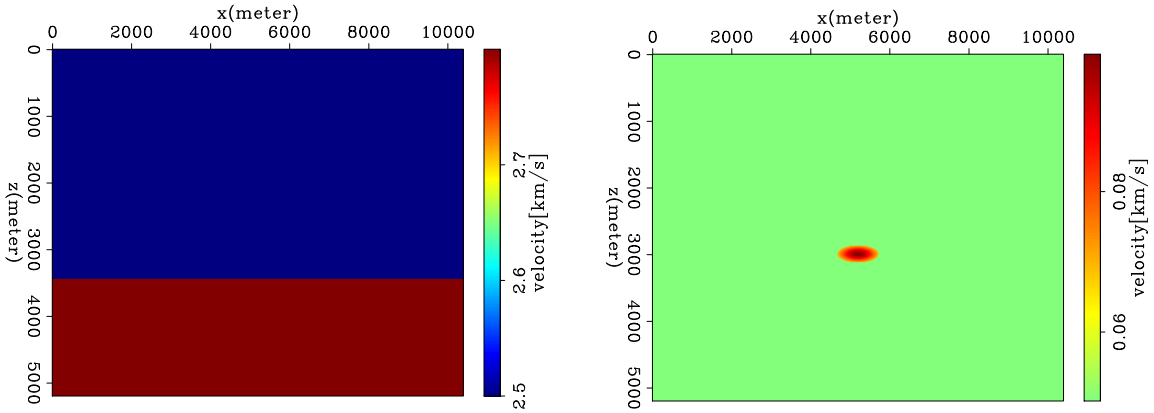

(a) (b)

Figure 2: (a) Background velocity model. (b) Velocity model perturbation. [**ER**]

Local time-lapse FWI solver

Next we construct a local solver for the 4D FWI problem. We demonstrate that we can predict the data residual at the surface and the gradient without requiring wave propagation in the overburden area, and use it to estimate the model perturbation.

Once we compute and recorded the perturbed wavefield at the virtual receivers, the data residual at the surface can be approximated by $\tilde{\mathbf{d}} = \mathbf{G}\tilde{\mathbf{p}}^{\text{syn}}(\mathbf{m})$ where $\tilde{\mathbf{p}}^{\text{syn}}(\mathbf{m})$ is estimated by local wave propagation around the reservoir. In Figure 5, we compare the true data residual and our estimated data residual. Most the data residual has been captured, despite observable artifacts. The reason is that our local wave propagation is not designed to capture all the perturbed wavefield. For example, the perturbed wavefield from the reflector beneath the boundaries is not included in our workflow.

We compare the FWI results from conventional FWI with our proposed workflow, and the results are shown in Figure 6. Both methods estimate the model perturbation properly. The results from our proposed workflow requires much less computational time comparing with the one from FWI with wave propagation in the whole subsurface, although they do not match completely.

Reducing the cost further by random phase encoding

Our final numerical experiment tests the feasibility to reduce the memory cost by random phase-encoding. In Figure 7a and 7b we show the FWI results with one realization of the random phase-encoding ($N_\alpha = 1$), with observable artifacts from the cross-talk between different shots. The cross-talk will reduce when multiple realizations of random phase-encoding are included in the objective function. In Figure 7c we show the results with $N_\alpha = 5$, and in Figure 7d we show the results with $N_\alpha = 20$. The results approach the one without phase-encoding (Figure 6b), when N_α is suffi-

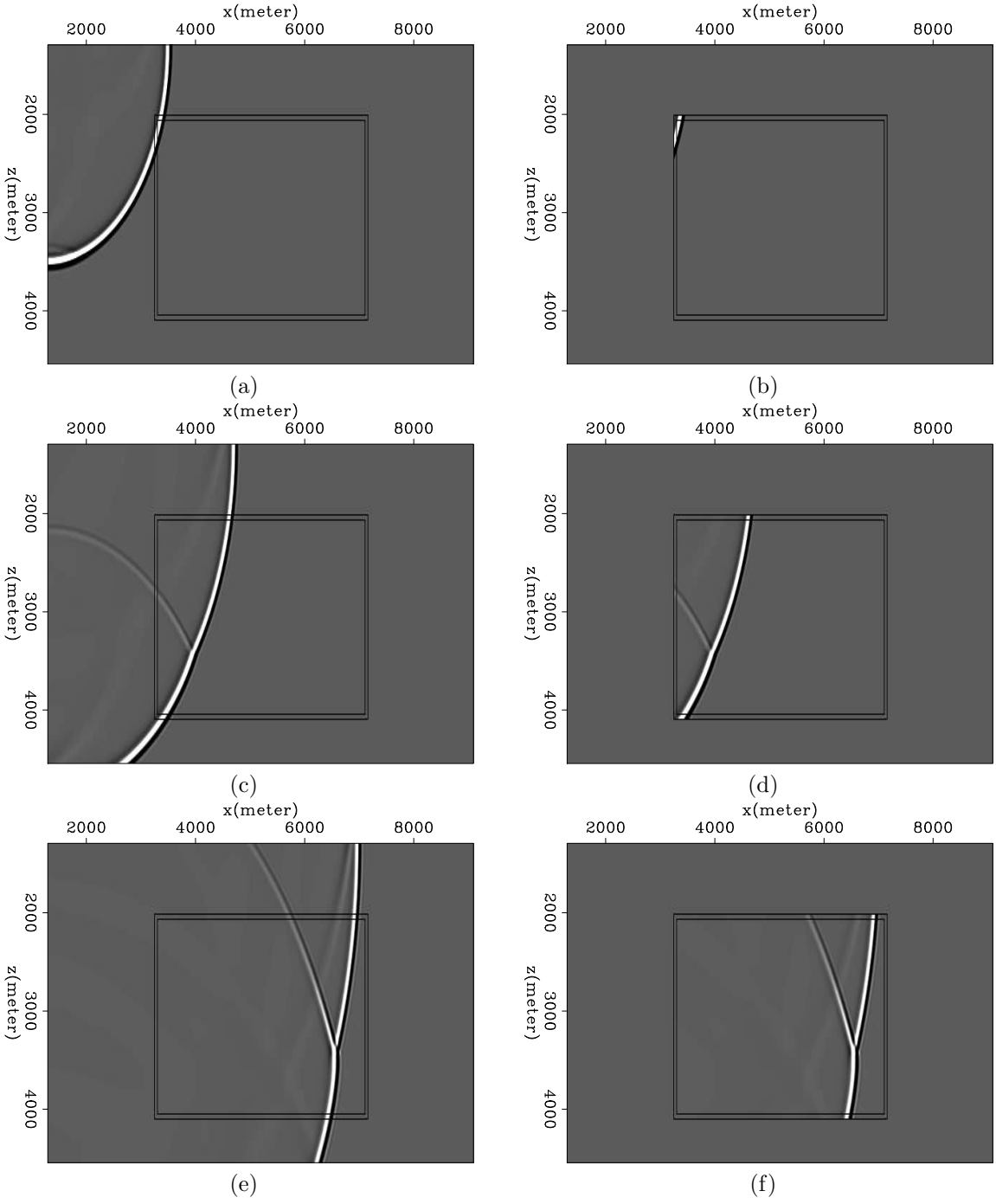

Figure 3: Left panel: (a), (c) and (e) are snapshots of wavefield by solving the wave equation in the whole subsurface. Right panel: (b), (d) and (f) are snapshots of wavefield by solving the wave equation around the reservoir with rejected boundaries. Black rectangles indicate the boundaries in which we save the wavefield. [**ER**]

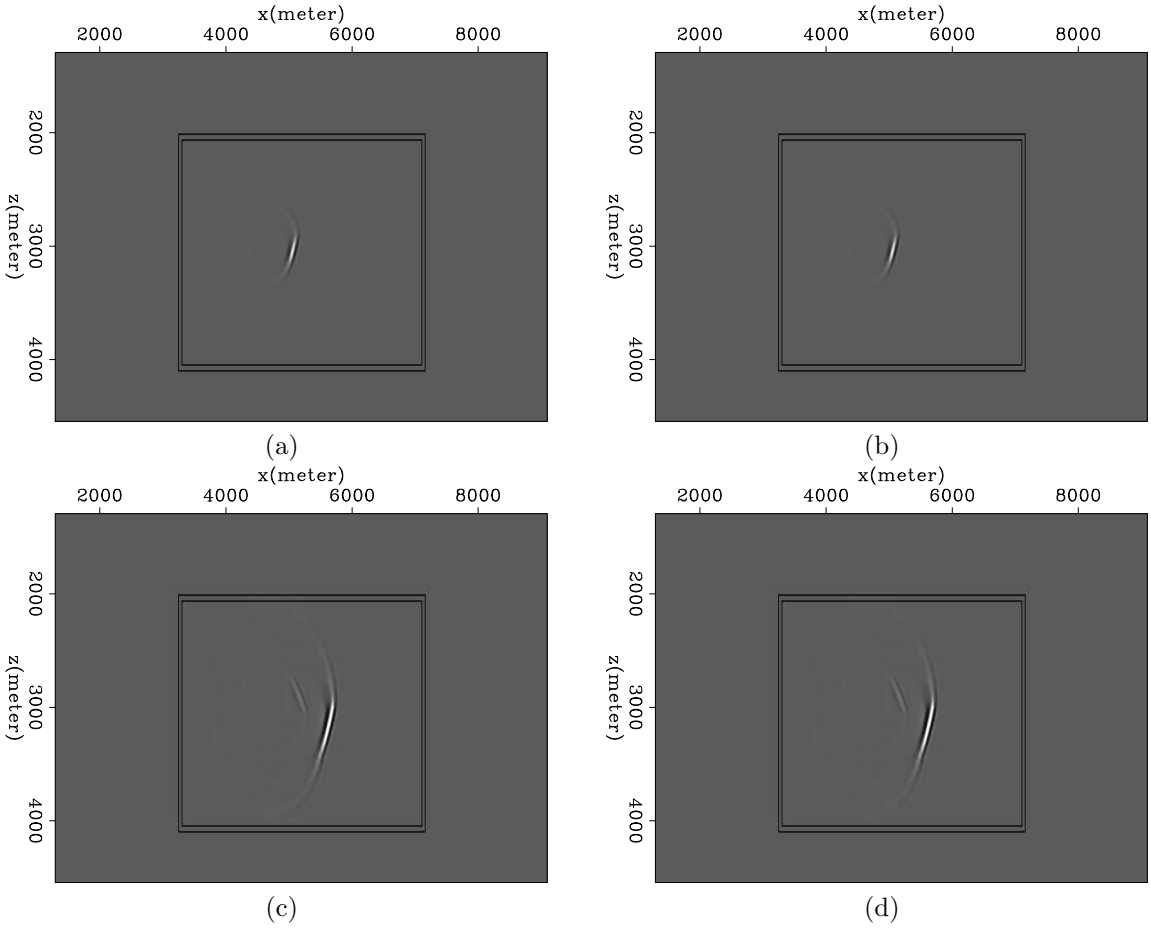

Figure 4: Left panel: (a) and (c) are snapshots of perturbed wavefield computed from the whole subsurface. Right panel: (b) and (d) are snaptshots of perturbed wavefield by solving the wave equation around the reservoir with rejected boundaries. [**CR**]

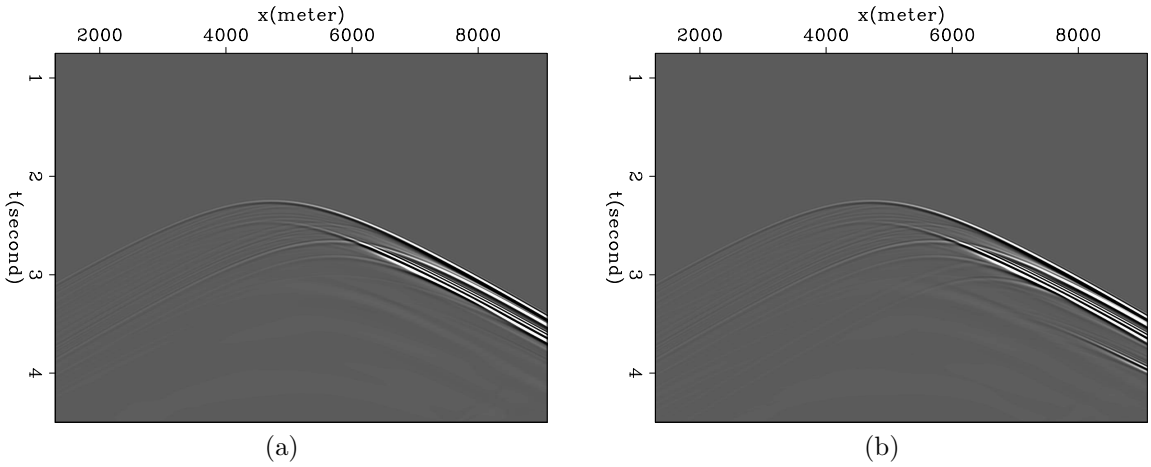

Figure 5: (a) True data residual.(b) Estimated data residual from local wave propagation around the reservoir, and pre-computed Green's function in the overburden. [**CR**]

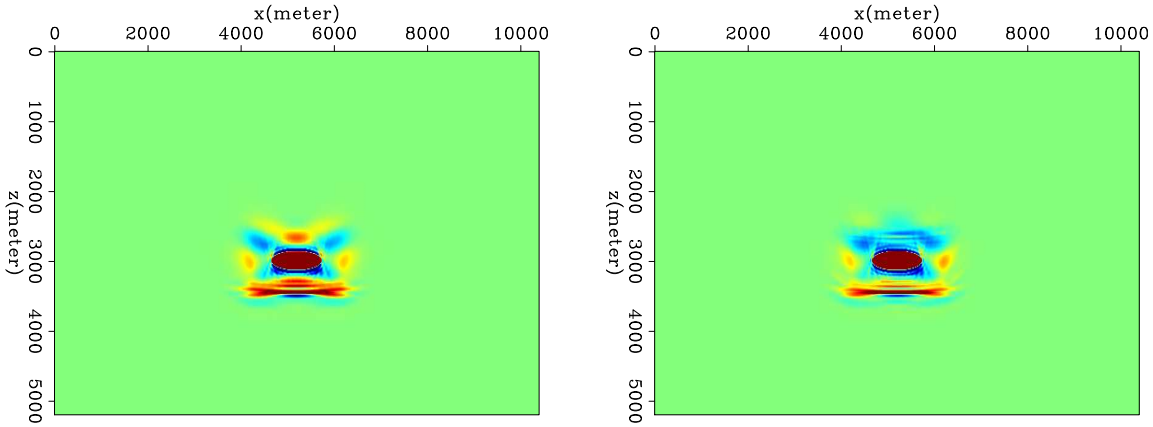

Figure 6: (a) Estimated model perturbation with conventional FWI method (wave propagation in the whole subsurface). (b) Estimated model perturbation using our proposed workflow (wave propagation around the reservoir). [**CR**]

ciently large, but much smaller than the number of shots N_s.

CONCLUSION

We show that by saving the wavefield at the boundary enclosing the reservoir, we can estimate the wavefield at the reservoir location after model perturbation. We eliminate the need to propagate the wavefield through the overburden area and therefore accelerate the FWI procedure. Random phase-encoding can be incorporated into our proposed workflow and has the potential to further reduce the computational cost.

REFERENCES

Borisov, D. and S. C. Singh, 2013, An efficient 3d elastic full waveform inversion of time-lapse seismic data using grid injection method, 954–958.

Clapp, R., 2008, Reverse time migration: Saving the boundaries: SEP Report 136.

Plessix, R. E., 2006, A review of the adjoint-state method for computing the gradient of a functional with geophysical applications: Geophysical Journal International, **167**, 495–503.

Robertsson, J. O. A. and C. H. Chapman, 2000, An efficient method for calculating finitedifference seismograms after model alterations: GEOPHYSICS, **65**, 907–918.

Tang, Y., 2011, Imaging and velocity analysis by target-oriented wavefield inversion: PhD thesis, Stanford University.

Tarantola, A., 1984, in the Acoustic Approximation: Geophysics, **49**, 1259–1266.

Tromp, J., C. Tape, and Q. Liu, 2005, Seismic tomography, adjoint methods, time reversal and banana-doughnut kernels: Geophysical Journal International, **160**, 195–216.

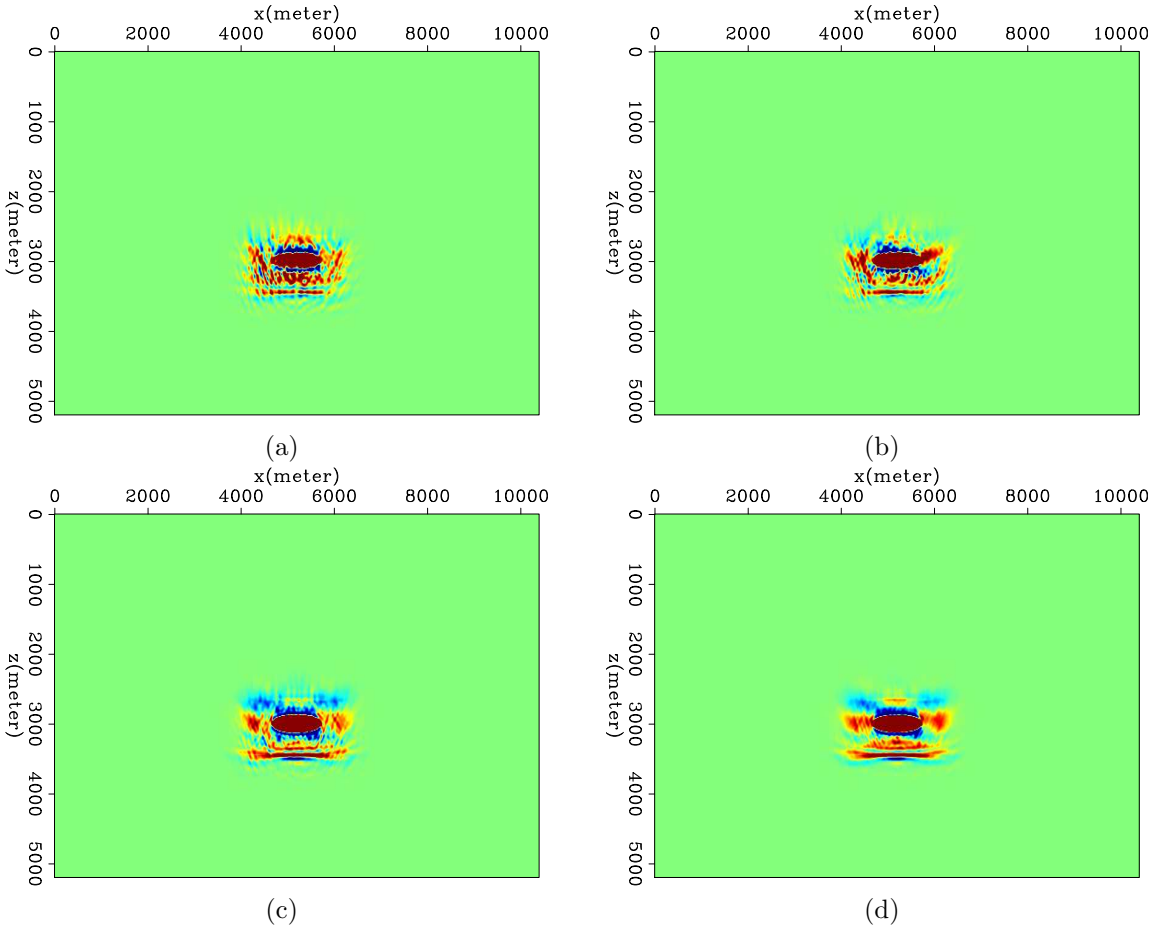

Figure 7: (a) estimated model perturbation with one realization of phase encoding $N_\alpha = 1$. (b) estimated model perturbation with another realization of phase encoding $N_\alpha = 1$. (c) estimated model perturbation with phase encoding $N_\alpha = 5$. (d) estimated model perturbation with phase encoding $N_\alpha = 20$. [**CR**]

Virieux, J. and S. Operto, 2009, An overview of full-waveform inversion in exploration geophysics: Geophysics, **74**, WCC1.

Willemsen, B., A. Malcolm, and W. Lewis, 2016, A numerically exact local solver applied to salt boundary inversion in seismic full-waveform inversion: Geophysical Journal International, **204**, 1703.